Feasibility study of detection of hazardous airborne pollutants using passive open-path FTIR

Segal-Rosenheimer M.[1], Dubowski Y.[1], Jahn C.[2], Schäfer K.[2], Gerl G.,[3] Linker R.[1]

[1]Department of Civil and Environmental Engineering, Technion-Israel Institute of Technology, Haifa, Israel.

[2]Institut für Meteorologie und Klimaforschung, Atmosphärische Umweltforschung (IMK-IFU) Karlsruhe Institute of Technology, Garmisch-Partenkirchen, Germany

[3]Helmholtz Center Munich, Institute of Soil Ecology, Scheyern, Germany

ABSTRACT

In recent years open-path FTIR systems (active and passive) have demonstrated great potential and success for monitoring air pollution, industrial stack emissions, and trace gas constituents in the atmosphere. However, most of the studies were focused mainly on monitoring gaseous species and very few studies have investigated the feasibility of detecting bio-aerosols and dust by passive open-path FTIR measurements. The goal of the present study was to test the feasibility of detecting a cloud of toxic aerosols by a passive mode open-path FTIR. More specifically, we are focusing on the detection of toxic organophosphorous nerve agents for which we use Tri-2-ethyl-hexyl-phosphate as a model compound. We have determined the compounds' optical properties, which were needed for the radiative calculations, using a procedure developed in our laboratory. In addition, measurements of the aerosol size distribution in an airborne cloud were performed, which provided the additional input required for the radiative transfer model. This allowed simulation of the radiance signal that would be measured by the FTIR instrument and hence estimation of the detection limit of such a cloud. Preliminary outdoor measurements have demonstrated the possibility of detecting such a cloud using two detection methods. However, even in a simple case consisting of the detection of a pure airborne cloud, detection is not straightforward and reliable identification of the compound would require more advanced methods than simple correlation with spectral library.

Keywords: Detection, aerosol cloud, remote sensing, toxic aerosols, passive infrared

1. INTRODUCTION

Developing measurement abilities of hazardous atmospheric aerosols is important in terms of environmental monitoring, risk assessment and crisis management. Open-path infrared instruments have been identified as a possible powerful tool for such tasks as they combine short measurement time, high-sensitivity and remote measurement capabilities, together with specific identification of the detected compounds. In the past several decades open-path Fourier transform infrared (FTIR) systems (active and passive) have demonstrated great potential and success for monitoring air pollution, [1] industrial stack emissions [2-4] and measurements of trace gas constituents in the atmosphere (e.g. [1, 5-7] and references therein). However, most of the past studies were focused mainly on monitoring gaseous species and only very few have investigated or tested the feasibility of detecting an airborne pollution cloud. The airborne materials investigated so far were bio-aerosols [8, 9],

Advanced Environmental, Chemical, and Biological Sensing Technologies VII,
edited by Tuan Vo-Dinh, Robert A. Lieberman, Günter Gauglitz, Proc. of SPIE Vol. 7673,
76730G · © 2010 SPIE · CCC code: 0277-786X/10/$18 · doi: 10.1117/12.850027

Saharan dust [10], and silicone oil as a model of dust particles [11], all of which were performed with an open-path FTIR setup in a passive detection mode.

Passive standoff detection of airborne pollutants has several advantages over an active set-up, including easiness of use, increased mobility and the elimination of prior and specific orientation set-up. However, its disadvantages include relatively low sensitivity and only partial understanding of the passive sensing scene and its parameterization. The latter is especially true for aerosol cloud detection, since parameterization of gaseous cloud scenes can be modeled quite simply in terms of gas spectroscopic parameters and radiation interactions (e.g. [5]). Aerosol cloud parameterization is much more complex since many physical properties of the specific material should be known a-priori (e.g. optical constants and size distribution), together with a more complex modeling of radiation interactions between the particles and the atmospheric layers. The goal of the present study was to test the feasibility of detecting a cloud of toxic aerosols by a passive mode open-path FTIR. Tri-2-ethyl-hexyl-phosphate was used as a model compound for either a nerve agent or an organophosphate pesticide. The first stage included the incorporation of a relatively detailed radiation model [12] to account for aerosol interactions with light, and the derivation of the aerosol parameters that were needed for the model (i.e. optical properties and size distributions). Theoretical calculations based on this model and various assumptions were made in order to better understand the signal that would be detected by an open FTIR system. The second stage of the study included a preliminary field campaign to measure the model material and to asses its detection probability.

2. THEORETICAL RADIATIVE MODEL

As mentioned above, there are significant differences between models of gaseous and aerosol clouds. One of the accepted models for passive standoff detection is illustrated in Figure 1. It describes the scene within the instrument line of sight (LOS) including three vertical layers, and a solid background, as adopted from Harig (2004) [5].

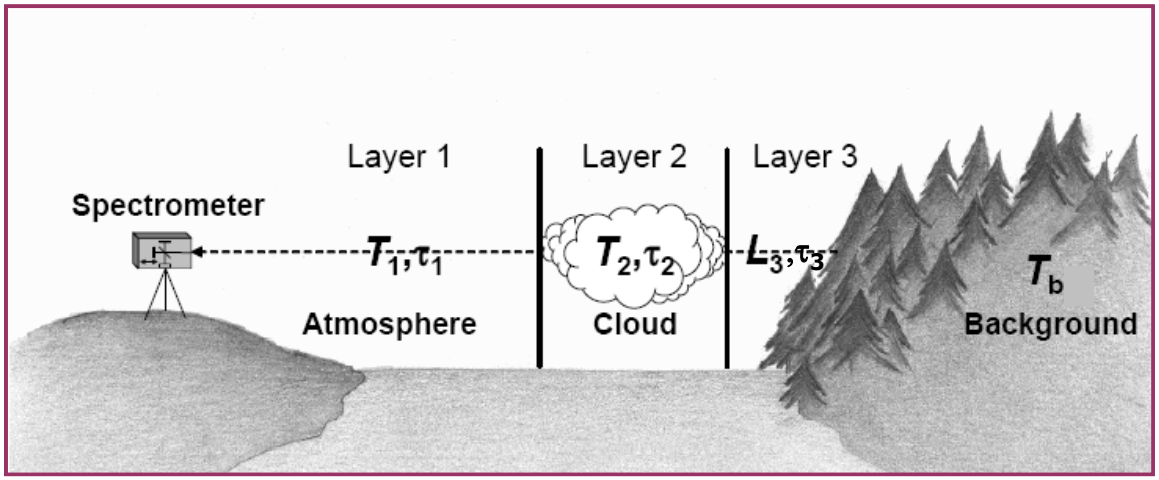

Figure 1: Schematic layout of a three layer atmospheric model for a passive standoff detection scene (reproduced from Harig, 2004[5]).

Equation 1 describes the wavelength dependent radiance at the spectrometer detector, $L_D(\lambda)$, based on the layered atmospheric model presented in Figure 1, where the second layer is a gaseous cloud:

$$[1] \quad L_D(\lambda) = L_1(\lambda) + \left(1 - \exp^{-\tau_2}\right) B_c(T_c, \lambda)\tau_1 + L_3(\lambda)\exp^{-\tau_2}\,\tau_1 + \varepsilon_b B_b(T_b, \lambda)\exp^{-\tau_2}\,\tau_1\tau_3$$

$L_1(\lambda)$ and $L_3(\lambda)$ represent the radiances of the layers in front and behind the pollutant cloud, and τ_1 and τ_3 represent the transmittance of these two atmospheric layers, respectively. B_c is the spectral radiance of a

blackbody at the temperature of the cloud T_c, τ_2 is the cloud's optical depth, and $\left(1-\exp^{-\tau_2}\right)$ is the cloud's emissivity. B_b is the spectral radiance of the background blackbody at temperature T_b, and ε_b is the background emissivity. In a gaseous cloud model, the cloud's optical depth τ_2 is a function of the gas absorption cross section, its concentration and the cloud size along the LOS. These parameters are relatively easy to measure in a laboratory and are usually known for many gaseous species of interest for environmental and hazard management applications. By comparison, a model for an aerosol cloud is much more complicated [9, 11, 12], and must include the specific aerosols properties and their interaction with ambient radiation. Equation 2 represents the full model for aerosol cloud detection using the scene shown in Figure 1 [5].

$$[2]\quad L_D(\lambda)=L_1(\lambda)+(1-\omega_0)\left(1-\exp^{-\tau_2}\right)B_c(T_c,\lambda)\tau_1+\varepsilon_1 B_c(T_c,\lambda)+\varepsilon_2 B_{sky}(T_{sky},\lambda)+L_3(\lambda)\exp^{-\tau_2}\tau_1 + \varepsilon_b B_b(T_b,\lambda)\exp^{-\tau_2}\tau_1\tau_3$$

In Equation 2 ω_0 is the clouds' single scattering albedo that represents the ratio between the mass scattering coefficient (α_{scat}) to the mass extinction coefficient (α_{ext}, which is the sum of the absorption and scattering coefficients). The second term in Equation 2 represents the direct thermal self emission of the cloud, while the third and fourth terms represent the internal scattering of the self thermal emission and the scattering of ambient radiation by the cloud, respectively. B_{sky} is the spectral radiance of a blackbody at the temperature of the sky T_{sky}. ε_1 and ε_2 are the emissivity components of each of the terms and are defined as [11]:

$$[3]\quad \varepsilon_1=\omega_0\int_0^{\tau_2}J_i(\tau)\exp^{-\tau}d\tau$$

and

$$[4]\quad \varepsilon_2=\omega_0\int_0^{\tau_2}J_e(\tau)\exp^{-\tau}d\tau$$

J_i and J_e are the internal and external source functions [12], and represent the integrated total radiance in all directions, which comes from the internal emission source and the external sky radiance source, respectively. Furthermore, in the aerosol case, τ_2, which is the cloud's optical depth, is a function of the mass extinction coefficient, α_{ext}, which is in turn a function of the aerosol complex index of refraction, and its size distribution. The mass extinction coefficient is calculated by using the Mie theory for the solution of a radiation field [13] that interacts with a sphere or an ensemble of spheres represented by a size distribution function. In order to obtain this solution, a-priori knowledge of the complex refractive index (i.e. optical properties) of the aerosol material and its size distribution is needed.

2.1 Optical constants derivation

Derivation of optical constants was performed using a method developed formally by Segal-Rosenheimer et al. [14]. In short, the method is based on the extraction of optical constants from small particles spectra, based on the fact that when the particles are small enough, their extinction cross section is proportional to their total volume and to a complex function containing the complex refractive index m ($m=n+ik$, where n and k are the real and imaginary index of refraction, respectively). Parallel measurement of the particles spectra and their size distribution is then used to extract both optical constants via the Kramers-Kronig Transform (KKT). In the present study we have generated various size distributions of liquid form of Tri-(2-ethyl-hexyl) phosphate (analytical grade, Sigma-Aldrich, 97% purity) by evaporating and condensing the pure material under different temperatures ranging from 30 to 60^{o}C. The generated droplets were then measured either for their size distribution (total volume) or for their spectral signal. Size distribution measurements were done using Scanning Mobility Particle Sizing (SMPS) system consisting of a Differential Mobility Analyzed (DMA, TSI model

3080L), and a Condensation Particle Counter (CPC, TSI model 3022A). Spectral measurements were performed with a long path IR gas cell (Infrared analysis Inc., model 6.2V, V=0.5L, optical path = 6 m) attached to an FTIR spectrometer (Bruker, Vertex 70), using MCT photovoltaic detector averaging 64 scans in a resolution of $2cm^{-1}$. Size distributions were log-normal with medians in the range 50-140 nm, with standard deviation 2nm. The retrieved optical constants are presented in Figure 2. As can be seen, the TOF has distinctive absorption bands in the Mid-IR spectral region, especially around the 1000 and 1400 cm^{-1} regions.

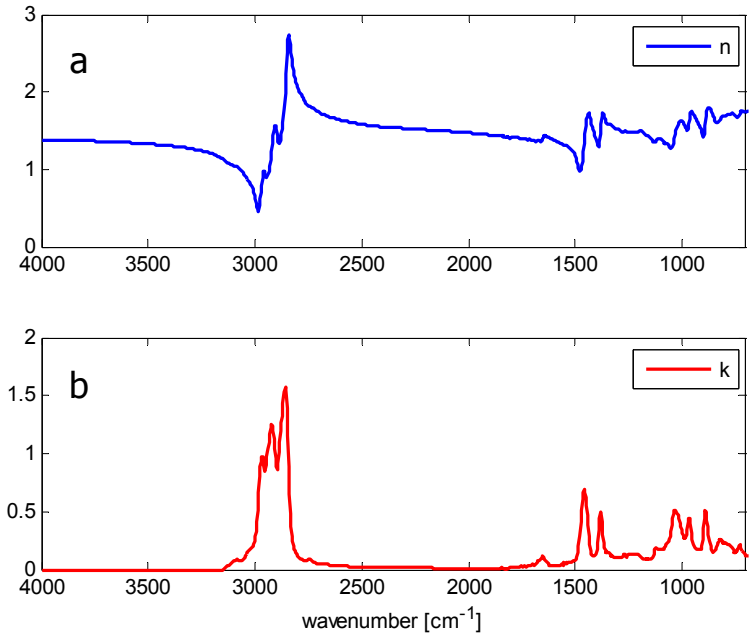

Figure 2: Complex refractive index components, (a) real refractive index, and (b) imaginary index of Tri-2-ethyl-hexyl-phosphate (TOF).

2.2 Model calculations

In order to evaluate the expected signal at the detector, calculations based on the theoretical radiative model and the derived optical constants presented above were performed. At first, we wanted to evaluate the total radiance at the detector, and compare it with the effective aerosol cloud signal. The total signal at the detector was derived in Equation 2. The aerosol cloud signal is represented by the difference between the total signal and the signal of a clean similar background with no cloud $L_0(\lambda)$:

$$[5] \quad L_0(\lambda) = L_1(\lambda) + L_3(\lambda)\tau_1 + \varepsilon_b B_b(T_b,\lambda)\tau_1\tau_3$$

The effective aerosol cloud signal is therefore:

$$[6] \quad \Delta L(\lambda) = \left(1-\exp^{-\tau_2}\right)\left[L_0(\lambda) - L_1(\lambda) - (1-\omega_0)B_c(T_c,\lambda)\tau_1\right] - \varepsilon_1 B_c(T_c,\lambda) - \varepsilon_2 B_{sky}(T_{sky},\lambda)$$

The total and effective TOF radiances are shown in Figure 3. These signals were calculated assuming that the aerosol cloud is very close to the detector (i.e. the first atmospheric layer was neglected and its transmittance was equal to 1), and has a log-normal distribution with a Count Median Diameter (CMD) of 0.2μm. It was further assumed that the blackbody temperatures of the aerosol cloud and of the third layer (beyond the cloud) were equal (288K). The background blackbody temperature was assumed to be 298K. The sky temperature is always lower than the cloud and background temperatures and was set to 263K. As shown in Figure 3, the

effective signal is more than one order of magnitude smaller than the total signal, emphasizing the limitations of passive detection of an aerosol cloud. Converting the radiance values into brightness temperature using the inverse Planck function shows that the maximal brightness temperature difference in the present case is 5K. Similar results were obtained by Ben-David and Ren [9] for a detection of a bio-aerosol cloud.

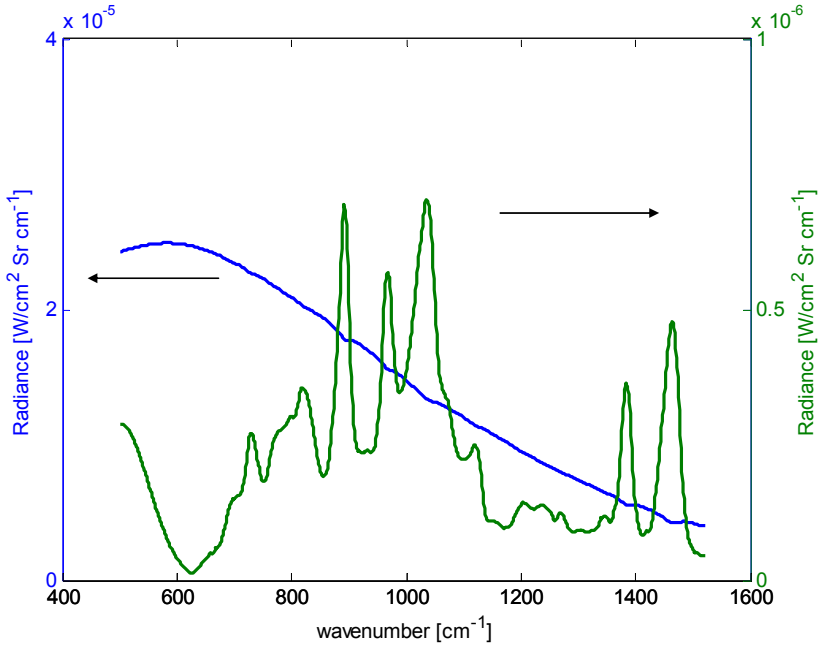

Figure 3: Total and effective radiances calculated using the theoretical model (Equations 2 and 6) for cloud and ambient temperatures of 288K, and background temperature of 298K.

As mentioned before, the actual size of the aerosols inside the cloud may vary, which in turns influences the detected radiance.
Aerosol size distribution is commonly described using a log-normal:

$$[7] \quad N = \frac{1}{\sqrt{2\pi}\ln(\sigma)D_p}\exp\left[\frac{\left(\ln D_p - \ln(CMD)\right)^2}{2\ln^2\sigma}\right]$$

N represents number of particles with diameter D_p, σ is the distribution geometrical standard deviation and CMD is the count (number) median diameter of the distribution. Figure 4 shows the TOF effective radiances (based on Equation 6) for various log-normal size distributions. As seen from the Figure, increasing the CMD parameter, which shifts the distribution towards larger particles, affects the effective signal in two ways. First, as the aerosol particles get larger, the overall radiance signal increases. Second, features that are not apparent in a spectrum of small particles become dominant for large particles. For example, when comparing the spectral signatures of CMD 0.2 μm and 7.2 μm it can be seen that next to the positive absorption bands appear negative ''dips'', which represent the effect of scattering of the ambient sky radiation by the aerosol cloud. Also, there seem to be a red shift for larger particles, a phenomenon that was observed in several other aerosol spectral investigations [14-16]. This understanding is important in terms of signal interpretation, and shows that the particles size distribution should be taken into account when comparing a measured signal with a reference ''library'' spectrum.

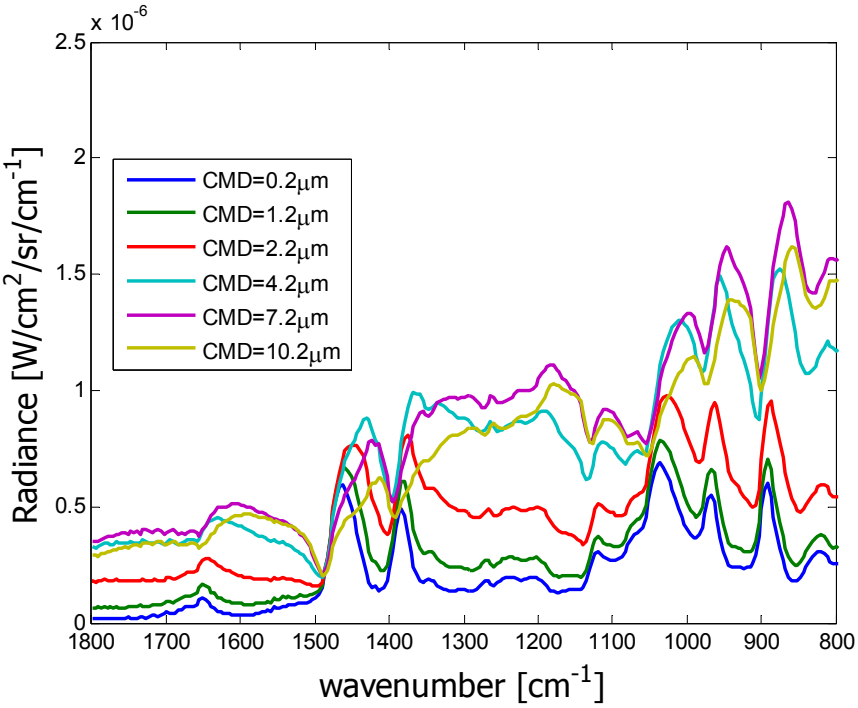

Figure 4: Effective TOF radiance calculated for various log-normal size distributions.

Figure 5 shows the calculated effective radiance for three log-normal size distributions at various temperature differences between the aerosol cloud and the solid background (background temperature was taken as higher than cloud at the positive ΔT values shown in Figure 5). As expected, when the temperature difference decrease the effective signal intensity also decreases. However, it can be seen that as the particle size distribution increases, the signal is still detectable, even when the aerosol cloud and background temperatures are equal. This effect is due to the addition of radiation at the detector that results from the aerosol cloud scattering effects. It can be concluded that, theoretically, an aerosol cloud with sufficiently large particles could be detected even at very low or no-temperature differences. This is in contrast to a gas cloud, for which if there is very small or no temperature difference between the cloud and the background, no spectral information can be obtained about the cloud [17].

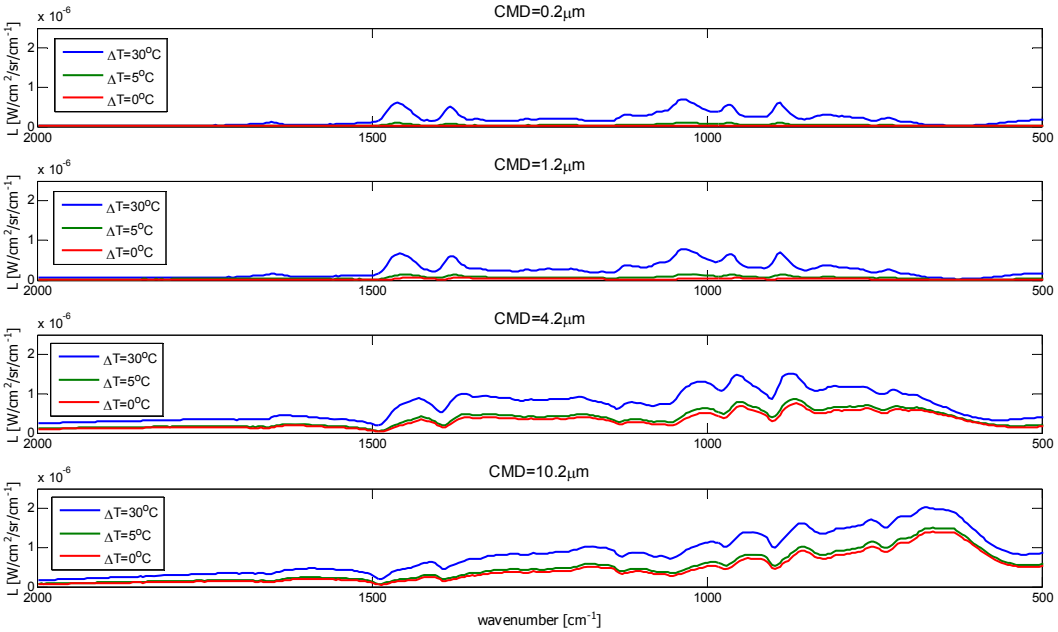

Figure 5: Effective TOF radiance calculated for various log-normal size distributions, and for various temperature differences between the aerosol cloud and the solid background (background temperature was higher for positive ΔT).

3. FIELD MEASUREMENTS

3.1 Measurements setup

A small scale field measurement was performed in order to test the theoretical model calculations and to test the feasibility of detecting an aerosol cloud in the field, under ambient conditions. The measurement site was located in research platform Scheyern of the Helmholtz Centre Munich which is located about 40 km North of Munich. The weather conditions were good throughout the two days of the experiment (which were held on 22-23/9/2009), with a clear sky and no wind. An open-path FTIR K300 with an MCT detector (range of 2-15μm) at a resolution of 4 cm^{-1} and a field of view of 0.3 mrad was used for the measurements. The instrument pointed toward a dense tree background. Radiance calibrations were made using blackbody measurements at 60°C and 200°C.

A TOF cloud was generated using five nebulizers (nitrogen blown) arranged in a row of approximately one meter. Due to the small cloud size generated with this method, the point of release was located 10 meters from the detector in order to make sure that the whole FOV would be covered during the cloud generation. The TOF liquid was an analytical grade material (Sigma-Aldrich, purity of 97%). The sprayed material size distribution was measured using a Grimm particle counter (model 1.108), and results are shown in Figure 6. As can be seen in the Figure, this measured distribution was not log-normal, but rather a Junge (exponential) distribution.

A typical experiment consisted of collection of background spectra for 15-30 minutes, followed by a release of the TOF for 5-10 minutes. The acquisition of the spectra was terminated 5-15 minutes after the cloud release.

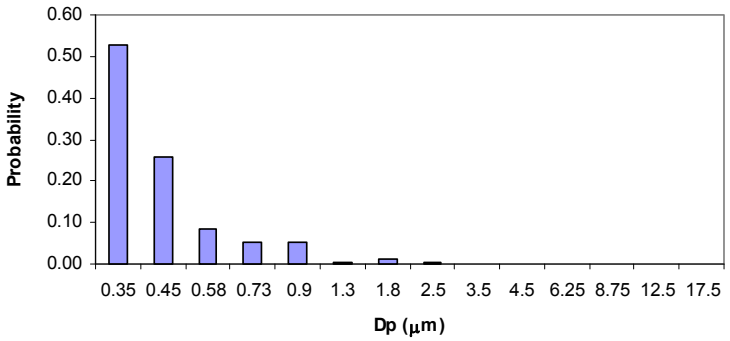

Figure 6: Measured probability distribution function of TOF sprayed during the experiments

3.2 Data analysis

The acquired data was recorded in instrument intensity units and was converted to radiance using the blackbody measurements mentioned above. These spectral signatures were analyzed using the **Orthogonal Subspace Projection (OSP)** method previously developed by Ben-David and Ren [9] and a novel approach detailed below.

The first algorithm used was the **Orthogonal Subspace Projection (OSP)** algorithm, which was adapted from the procedure developed by Ben-David and Ren [9]. In short, this method uses a statistical spectra subtraction approach canceling the contribution of the background (environmental) signal and extracting the pollutant signal. In this procedure, the measured dataset is divided into two parts and the clean background scans (before spraying the cloud) are used to characterize the background signal. Principal component analysis (PCA) is performed on this subset to determine the spectral components (or "directions") that describe best the background spectra (usually only one or two principal components are retained). Those components are then used to construct an orthogonal subspace projection (OSP) operator. Clearly, applying this operator to the background signal itself results in an almost zero signal, so that a non-zero projected signal can be associated with the presence of an aerosol cloud. In principle, Ben-David and Ren [9] suggested that the method can be also used without a-priori knowledge of the background, such that the PCA will be done on all measurements data. However, this is only possible when the cloud corresponds to a very small temporal portion of the total scene, which is not the case here.

Figure 7 shows the result of such analysis on two of the spectra recorded during the first experiment. In the Figure, the average background signal ± 1 standard deviation interval are shown, together with the cloud signal after 1 and 2 minutes (where each spectrum measurement took 13 seconds). Although bands around 1000-1100, 1400, and 1500 cm^{-1} can be seen emerging, the difference between the projected signals before and after the cloud release is not very large.

Figure 8 shows the correlation between the projected spectra and the reference spectrum that was calculated using the theoretical models presented in Section 2.2, given the measured size distribution shown in Figure 6. As shown in the Figure, the correlation value increased after cloud spraying and remained high throughout the time of the cloud spraying. Also it can be seen that the high correlation values remained even after the stop of the spraying, which may indicate that there was not enough time for the cloud to disperse, due to the no-wind conditions that prevailed during the experiment. As each measurement took 13 seconds, the last measurement was taken only four minutes after the cloud release. In general, the correlation value during the cloud spraying was around 0.7, which is lower than values previously reported for this method (around 0.82 by Ben-David [8]). A possible explanation for this relatively low value could be that the material used in this study has sharp spectral features, in the thermal-IR region, in contrast to previously tested materials such as bio-aerosols [8] and silicon oil droplets [11] which present very broad bands in this spectral region.

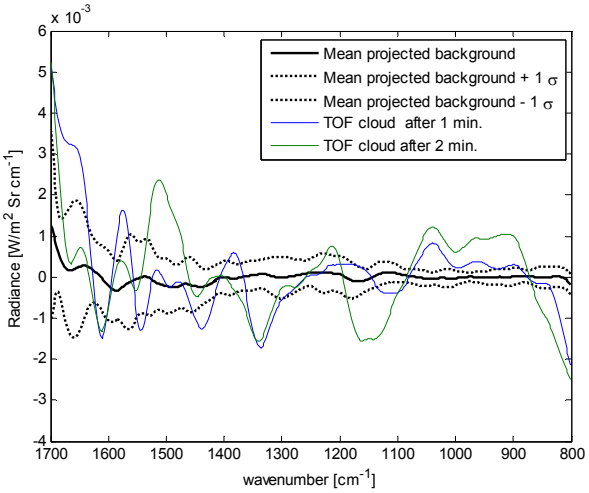

Figure 7: Signals obtained after applying the OSP operator to the background spectra (before the cloud release – background only) and to the cloud spectra.

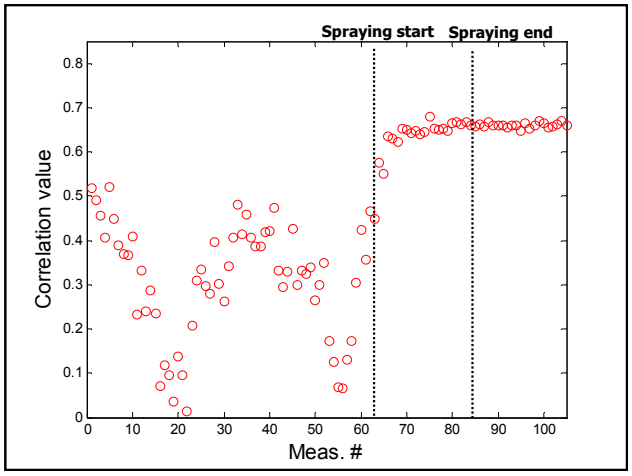

Figure 8: Correlation values between the TOF reference spectrum and the measured data after applying the OSP procedure as detailed in text.

The second analysis was performed using a novel approach termed the **Time Correlation Filter (TCF)** developed by us specifically to try to separate the aerosol signal from the ambient signal. The basic assumption of the method is that, over time, the radiance signals at wavelengths associated with the background should behave differently than the radiance signals at wavelengths associated with the aerosols. In this method, the analysis is performed repeatedly on a moving window signal (containing n consecutive measurements) without a-priori separating the clean background measurements from the ones collected in the presence of the cloud. For each window, the first step of the method consists of calculating the λ-by-λ correlation matrix that represents the correlation values between the radiances at each of the wavelengths. Wavelengths that are very strongly correlated (in this study, correlation coefficient above 0.95) are considered as candidates for defining the background signal. However, this correlation test by itself is not sufficient since wavelengths that are highly correlated with only one or few other wavelengths are retained. Therefore, the histogram of the number of high correlations is calculated and only the wavelengths above the third quartile are selected. After determining the set of the background wavelengths (denoted as λ_{bkg}), Principal Component Analysis (PCA) is performed on the n-by-λ_{bkg} "background" subset matrix to capture the main trends in the background variations over time. A

projection operator orthogonal to the first principal components (which capture the main trends) is then calculated as [9]:

$$[8] \quad P_U^{orth} = I - U\left(U^T U\right)^{-1} U^T$$

where U denotes the matrix that contains the selected principal components and *I* is the identity matrix of appropriate dimensions. Since the P_U^{orth} operator is orthogonal to the background trends, after applying this operator to all the signals of the window, the signals whose evolution over time can be explained by background changes will be close to zero and only the signals with different temporal evolutions will remain.

The results obtained by applying the TCF procedure to the data collected during the second experiment are presented in Figure 9. Procedure was done using two principal components in U to describe the background. The Figure shows two segments of the analysis, containing a window of measurements before (Figure 9a) and after cloud spraying (Figure 9b). As shown in Figure 9a, the projected intensities at the wavelengths identified as "background" are very small, while the projected intensities of the other wavelengths show various trends with time (Figure 9b). Figure 9 shows the whole wavelength range, and hence makes it difficult to distinguish between the different spectral regions and their behavior. For this purpose, more detailed results are shown in Figure 10 where the same signals in Figure 9 were grouped (and averaged) according to the various spectral features of the TOF. It can be clearly seen that the greatest change occur at measurement number 82, which corresponds to the cloud release start. The bands ranging between 930-1100 cm^{-1} show the greatest change in time for this case.

An additional very strong indicator for the cloud detection is the number of wavelengths identified as “background”. This can be seen in Figure 11, which shows the number of wavelengths that were selected to describe the background in each window. As expected, many wavelengths were included in the background signal before the cloud release (until measurement 82), and as the cloud appeared (at measurement 82), the number of wavelengths included in the background signal decreased dramatically from 260 to 60, indicating that many wavelengths now are representing the cloud signal itself.

The results obtained by using the TCF method look promising in terms of detecting the appearance of the cloud and in identifying some of the important spectral bands, which are associated with the specific material. However, these are still preliminary results, as there are many parameters that affect this analysis (e.g. initial correlation thresholds and the number of principal components selected to describe the background signal). Longer measurements would be required in order to conduct a rigorous statistical analysis regarding the difference between the background and cloud signals and the effect of the parameters in this method.

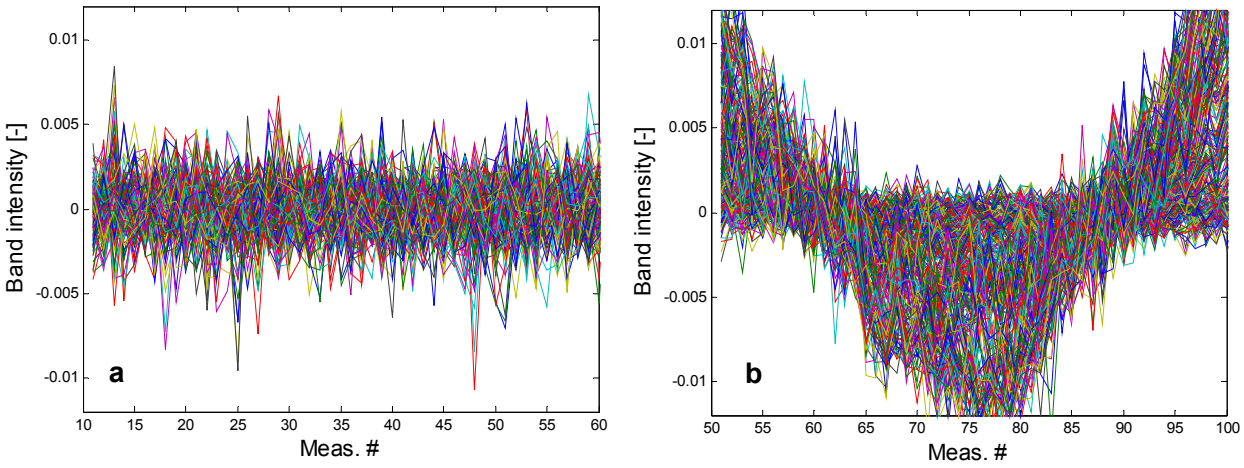

Figure 9: Temporal evolution of (a) the projection of the signals recorded before the cloud release and (b) during the cloud release.

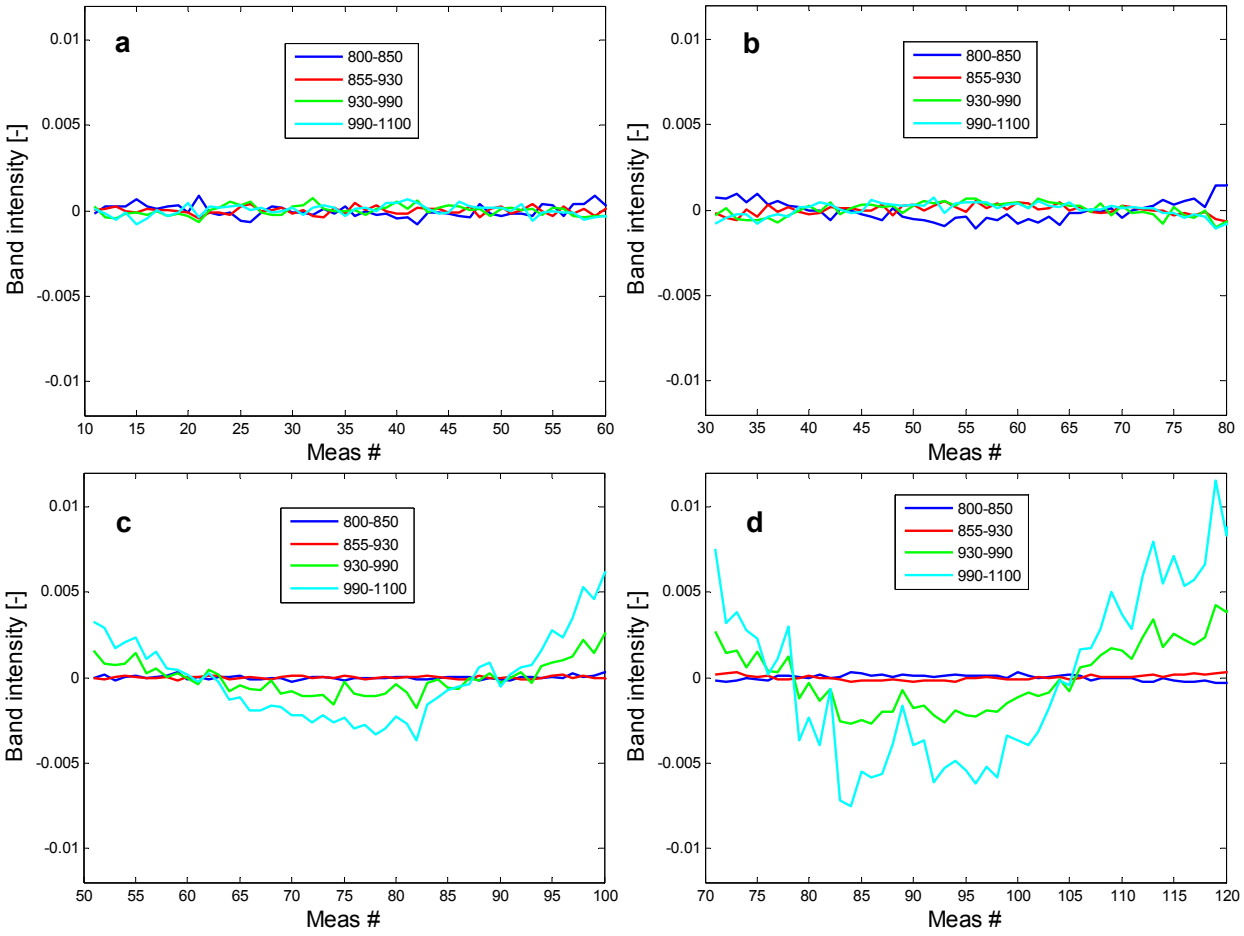

Figure 10: Temporal evolution of the clustered and averaged bands intensity for some of the wavelengths range shown in Figure 9. The four frames correspond to various time windows. The cloud release started at measurement 82. The legend indicates the intervals in which the projected signals were averaged.

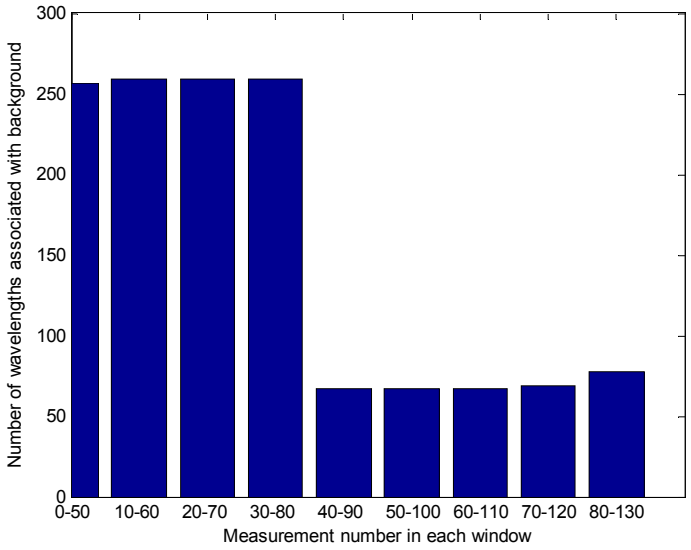

Figure 11: Number of wavelengths selected to represent the background signal in each window section of the signal.

4. CONCLUSIONS

In this paper we have shown a theoretical model for predicting aerosol cloud signal at a passive open-path FTIR detector. We have shown that aerosol properties such as the specific material's optical properties (i.e. complex refractive index) and their size distribution affect the effective signal at the detector. Hence, it is important to provide this data a-priori in order to better simulate and match the theoretical signal to a measured one. Also, detection of aerosol cloud is feasible even under very small temperature difference, in contrast to a gas cloud signal. From the analyses done on our preliminary field campaign measurements we have shown that the use of the Orthogonal Subspace Projection method (OSP) can detect the appearance of a cloud, and the measured signal can be compared with a pre-defined reference spectrum for material identification. However, it was shown that in the present case the signal difference between the projected background and the signal itself was small, a problem that can affect the strength of such analysis. Also, relatively low correlation values were obtained (around 0.7), which raises questions regarding the applicability of the method for materials with sharp spectral features. The novel method presented here, Time Correlation Filter (TCF) appeared to give promising results in terms of the temporal detection of the cloud release. Nevertheless, a more robust and comprehensive testing incorporating a larger dataset is required to statistically confirm the difference between the signals. The main advantage of this method is that it does not require any a-priori knowledge regarding the background and the timing of the cloud appearance. In the future new spectroscopic developments such as spatial heterodyne spectroscopy [18]can offer improved applications for passive aerosol detection.

5. ACKNOWLEDGEMENTS

The authors would like to thank the Technion Research Fund and the Minerva Fellowship Program (Israel-Germany research relations), which allowed to perform field experiments in Germany. Michal Segal-Rosenheimer acknowledges the financial support of the Levi Eshkol scholarship of the Israeli Ministry of Science and the financial support of the SPIE that enabled her attend the Conference and present her work.

6. REFERENCES

[1]. Hong DW, Gwi Suk Heob, Jin Seok Hanc,Cho SY. Application of the open path FTIRwith COL1SB to measurements of ozone and VOCs in the urban area. Atm. Environ. 2004. 38:5567-5576.

[2]. Childers JW, Jr ELT, Harris DB, D.A. Kirchgessner, Clayton M, Natschke DF,Phillips WJ. Multi-pollutant concentration measurements around a concentrated swine production facility using open-path FTIR spectrometry. Atm. Environ. 2001. 35:1923-1936.

[3]. Haus R, Schäfer K, Bautzer W,Heland JM, H., Bittner, H., Eisenmann, T. Mobile FTIS-Monitoring of Air Pollution. Appl. Opt. 1994. 33:5682-5689.

[4]. Yokelson RJ, Susott R, Ward DE, Reardon J,Griffith D. Emissions from smoldering combustion of biomass measured by open-path Fourier transform infrared spectroscopy. J. Geophy. Res. 1997. 102:18865-18877.

[5]. Harig R. Passive remote sensing of pollutant clouds by FTIR spectrometry: Signal-to-noise ratio as a function of spectral resolution. Appl. Opt. 2004. 43:4603-4610.

[6]. Kuttler W,Straburger A. Air quality measurements in urban green areas—a case study. Atm. Env. 1999. 33:4101-4108.

[7]. Kuttler W, T. Lamp,Weber K. Summer air quality over an artificial lake. Atm. Env. 2002. 36:5927-5936.

[8]. Ben-David A. Remote detection of biological aerosols at a distance of 3 km with a passive Fourier transform infrared (FTIR) sensor. OPTICS EXPRESS 2003. 11:418-429.

[9]. Ben-David A,Hsuan R. Detection, identification, and estimation of biological aerosols and vapors with a Fourier-transform infrared spectrometer. Appl. Opt. 2003. 42:4887-4900.

[10]. Turner DD. Ground-based infrared retrievals of optical depth, effective radius, and composition of airborne mineral dust above the Sahel. Journal of Geophysical Research-Atmospheres 2008. 113.

[11]. Agassi E, RONEN, A. NS. Discrimination between natural dense dust clouds with IR spectral measurements. International Journal of High Speed Electronics and Systems 2008. 18:647-660.

[12]. Sutherland RA. 2002. Determination and Use of IR Band Emissivities in a Multiple Scattering and Thermally Emitting Aerosol Medium. *In* Laboratory SLADIEPD-AR (ed.).

[13]. Bohren CF,Huffman DR. Absorption and scattering of light by small particles 2004. Weinheim. Wiley-VCH.

[14]. Segal-Rosenheimer M, Dubowski Y,Linker R. Extraction of optical constants from Mid-IR spectra of small aerosol particles. J Quant Spectrosc Radiat Transfer 2009. 110:415-426.

[15]. Toon O, Pollack J,Khare B. The optical constants of several atmospheric aerosol species: Ammonium sulfate, aluminum oxide, and sodium chloride. J. Geophys. Res. 1976. 81:5733.

[16]. Weis DD,Ewing EG. Infrared spectroscopic signatures of (NH4)2SO4. J. Geophys. Res. 1996. 101:18709-18720.

[17]. Beil A, Daum R, Matz, G., Harig, R. 1998. Presented at the Spectroscopic Atmospheric Environmental Monitoring Techniques.

[18]. Englert C, Babcock D., Harlander J., Long-wave IR sensing using spatial heterodyne spectroscopy, SPIE Newsroom 2009.10.1117/2.1200912.002532.